

Improved Deep Learning Methods for Large-Scale Dynamic Portfolio Choice

Jeonggyu Huh¹, Hyeng Keun Koo², and Jaegi Jeon^{*3}

¹Department of Mathematics, Sungkyunkwan University, Republic of Korea

²Department of Financial Engineering, Ajou University, Republic of Korea

³Graduate School of Data Science, Chonnam National University, Republic of Korea

January 23, 2025

Abstract

We present a Pontryagin-Guided Direct Policy Optimization (PG-DPO) method that scales dynamic portfolio choice—including consumption and multi-asset investment—to tens of thousands of risky assets. By combining neural-network controls with Pontryagin’s Maximum Principle (PMP), we avoid intractable dynamic programming (DP) grids, which traditionally cannot handle more than six assets in practice. Instead of approximating the value function (as in deep backward stochastic differential equation (BSDE) methods), we track a policy-fixed adjoint process and align each gradient update with continuous-time PMP conditions. A “one-shot” variant deploys Pontryagin controls after a brief warm-up, often achieving 100–1,000-fold accuracy improvements over naive baselines. Crucially, on modern GPUs, 100,000 iterations typically take under an hour, while a few thousand iterations (often just 1–2 minutes) already yield near-optimal solutions for portfolios with thousands of assets. Numerical experiments confirm consistency with one-asset Merton benchmarks and tractability up to 10,000 assets, surpassing the longstanding DP-based limit of fewer than seven. This enables truly large-scale continuous-time portfolio optimization.

1 Introduction

Dynamic portfolio choice—how an investor should optimally allocate wealth among multiple assets and consume over time under uncertainty—is a cornerstone of

*Corresponding Author: jaegijeon@jnu.ac.kr

modern finance. Classic studies by Samuelson (1975) and Merton (1969, 1971) pioneered both continuous-time and discrete-time frameworks in which investors balance growth, risk, and consumption. Under certain strong assumptions (for instance, complete markets or specific functional forms), researchers have even derived (semi-)closed-form solutions (e.g., Kim & Omberg, 1996; Liu, 2007). However, many real-world features—including return predictability, stochastic volatility, and trading constraints—invalidate these assumptions and necessitate more flexible numerical techniques.

A large body of work has sought to refine or extend these models by introducing time-varying parameters or incomplete markets, typically relying on dynamic programming (DP). Unfortunately, DP-based methods often suffer from the curse of dimensionality as the number of risky assets grows. For example, Campbell & Viceira (1999, 2001); Campbell et al. (2003) incorporate multiple state variables (e.g., dividend yields, interest rates) but must limit the number of risky assets (below seven) for tractability. Empirical studies by Balduzzi & Lynch (1999), Lynch & Balduzzi (2000); Lynch (2001), and Brandt et al. (2005) add transaction costs or learning about returns, yet still focus on relatively small portfolios. Sophisticated computational methods (Buraschi et al., 2010; Garlappi & Skoulakis, 2010; Jurek & Viceira, 2011) cannot fully escape the exponential blow-up in high-dimensional DP problems.

In response, we develop a scalable framework that accommodates *thousands* of assets while preserving a continuous-time perspective on consumption and investment. Specifically, we show how a Pontryagin-Guided Direct Policy Optimization (PG-DPO) scheme, combined with a novel “one-shot” training approach, enables us to solve portfolio problems with up to 10,000 assets—a major leap beyond the traditional limit of fewer than seven. Empirically, we find that using this one-shot variant yields accuracy improvements on the order of 100–100,000 times relative to a naive PG-DPO baseline. In practice, on a modern GPU (e.g., an RTX 4090), 1,000 gradient updates (sufficient for highly accurate solutions) typically complete in under an hour, and just a few thousand iterations (taking 1–2 minutes) often suffice to produce near-optimal performance even for thousands of assets. Although we focus on a continuous-time setting in the spirit of Merton (1971), the core concepts naturally extend to discrete-time frameworks with minor modifications. Moreover, while our examples emphasize consumption and portfolio choice, adding features such as wages or other cashflow components is straightforward within the same neural-policy architecture.

Recently, machine-learning-based tools for stochastic control (including deep BSDE methods (e.g., Han et al., 2018; Weinan, 2017), physics-informed neural networks (PINNs) (Raissi et al., 2019), and reinforcement learning (RL) (Dai et al., 2023)) have shown promise in principle. However, these methods typically focus on

value-based approaches: they approximate a value function (or solve a PDE) and then derive a policy. In high-dimensional settings with thousands of assets—and especially when consumption is added—the value surface can become prohibitively complex. Even small errors in value estimation can lead to large deviations in the induced policy, making it difficult to achieve accurate controls as dimension grows. Indeed, deep BSDE and PINN approaches often target single-asset or simpler PDE problems (e.g. basic Black–Scholes), and model-free RL has been tested mostly on small-scale tasks with few assets. Meanwhile, traditional DP can handle up to six assets in certain empirical studies (Lynch, 2001) but quickly becomes infeasible beyond that. These factors leave a significant gap in the ability to handle truly large-scale, continuous-time portfolio problems without sacrificing the underlying optimal-control framework. In contrast, we adopt a *policy-centric* approach that bypasses extensive value-function approximation. Instead, we enforce Pontryagin conditions directly via neural-network policies, allowing the method to remain tractable and consistent even as the number of assets rises to the thousands.

Our primary methodological contribution is to illustrate how large-scale dynamic portfolio problems can be solved via *direct stochastic-gradient policy optimization*, obviating the need for an intractable DP grid. Concretely:

1. We develop **PG-DPO** (Pontryagin-Guided Direct Policy Optimization), a scheme that parametrizes both consumption and portfolio decisions with neural networks, mapping the investor’s wealth (and any additional state variables) to allocation and consumption rates in a flexible, scalable manner.
2. We introduce a **PG-DPO-OneShot** variant that, after a brief warm-up, harnesses Pontryagin-adjoint information. By estimating costates through backpropagation-through-time (BPTT), we directly deploy the resulting Pontryagin controls, bypassing further training loops. This “one-shot” procedure can boost accuracy by up to five orders of magnitude relative to a naive approach.
3. We demonstrate that our method remains robust at extreme scales—supporting up to 1,000 risky assets in a single training loop—while delivering minimal errors and aligning closely with known closed-form solutions in lower-dimensional settings.

Although we do not incorporate real-world market data or extensive exogenous factors here, the framework naturally accommodates richer settings. In particular, it can be extended to incorporate constraints—such as borrowing limits, transaction costs, or short-selling restrictions—by suitably modifying the forward SDE and the Pontryagin Hamiltonian. Our core aim, however, is to establish that large-scale, continuous-time dynamic portfolio choice with up to 10,000 assets is computationally feasible under this unified policy-optimization approach.

In Section 2, we formulate the multi-asset Merton problem with both consumption and investment. Section 3 then applies Pontryagin’s Maximum Principle (PMP) to derive adjoint processes and characterize the optimal controls. Next, Section 4 develops our neural-network-based algorithm, showing how backpropagation-through-time (BPTT) enforces PMP conditions in a scalable fashion. Section 5 presents numerical experiments demonstrating the method’s performance across a range of dimensions (up to 10,000 assets). Finally, Section 6 concludes and discusses possible extensions for large-scale, continuous-time portfolio optimization.

2 Multi-Asset Continuous-Time Portfolio Problem

In this section, we present a multi-asset version of Merton’s classic portfolio problem (Merton, 1971), wherein an investor allocates wealth among multiple risky assets and a risk-free asset while also consuming continuously. Unlike the single-asset case, the presence of multiple (potentially correlated) assets with distinct drifts and volatilities leads to richer portfolio strategies and more challenging solution methods. In particular, although the *wealth* itself remains one-dimensional, the *investment decision* can span multiple dimensions, reflecting the investor’s choices across different risky assets.

2.1 Market Model and Wealth Dynamics

Suppose there are n risky assets, whose prices at time t are denoted by the vector $\mathbf{S}_t = (S_t^{(1)}, S_t^{(2)}, \dots, S_t^{(n)})^\top$. We assume each $S_t^{(i)}$ follows a geometric Brownian motion under an n -dimensional *standard* Brownian motion $\mathbf{W}_t = (W_t^{(1)}, \dots, W_t^{(n)})^\top$. Let $\boldsymbol{\mu} \in \mathbb{R}^n$ be the vector of (constant) drifts, and let $\Sigma \in \mathbb{R}^{n \times n}$ be the (constant) *covariance matrix*, assumed positive definite. Although Σ fully describes the (co)variances and correlations among assets, it is often convenient in *implementations* or *simulation* to use a volatility matrix \mathbf{V} satisfying $\Sigma = \mathbf{V} \mathbf{V}^\top$, where \mathbf{V} can be taken as the (upper-triangular) Cholesky factor of Σ . Then each asset’s price evolves via

$$d\mathbf{S}_t = \text{diag}(\mathbf{S}_t) \left(\boldsymbol{\mu} dt + \mathbf{V} d\mathbf{W}_t \right), \quad \mathbf{S}_0 = \mathbf{s}_0 > \mathbf{0},$$

where \mathbf{W}_t remains an n -dimensional *standard* Brownian motion (i.e. with independent components), and all asset correlations are captured by \mathbf{V} . Additionally, there is a risk-free asset B_t with constant rate r , satisfying $dB_t = r B_t dt$. Let X_t be the investor’s total wealth at time t . The investor continuously chooses a consumption rate $C_t \geq 0$ and an \mathbf{n} -dimensional investment proportion $\boldsymbol{\pi}_t$, whose i -th

component $\pi_t^{(i)}$ represents the fraction of current wealth X_t allocated to the i -th risky asset. The remaining fraction $(1 - \sum_i \pi_t^{(i)})$ may be invested in the risk-free asset (depending on whether short sales or leveraged positions are allowed). Then X_t evolves according to

$$dX_t = \left[r X_t + X_t \boldsymbol{\pi}_t^\top (\boldsymbol{\mu} - r \mathbf{1}) - C_t \right] dt + X_t \boldsymbol{\pi}_t^\top \mathbf{V} d\mathbf{W}_t, \quad X_0 = x_0 > 0, \quad (1)$$

where $\mathbf{1}$ is the all-ones vector in \mathbb{R}^n . Admissibility requires that $\boldsymbol{\pi}_t$ and C_t be adapted processes keeping X_t nonnegative almost surely.

Although (1) does not admit a simple closed-form solution when $\boldsymbol{\pi}_t$ and C_t vary over time, we can obtain a *local* exponential solution on any short interval $[t, t + \Delta t]$ by temporarily freezing $\boldsymbol{\pi}_s = \boldsymbol{\pi}_t$ and $C_s = C_t$. Define

$$\beta := r + \boldsymbol{\pi}_t^\top (\boldsymbol{\mu} - r \mathbf{1}), \quad \alpha := \frac{C_t}{X_t}.$$

Then, for Δt small,

$$\frac{dX_s}{X_s} \approx (\beta - \alpha) ds + (\boldsymbol{\pi}_t^\top \mathbf{V}) d\mathbf{W}_s, \quad s \in [t, t + \Delta t].$$

By applying Itô's Lemma to $\ln(X_s)$, one obtains an additional *Itô correction* of $-\frac{1}{2} (\boldsymbol{\pi}_t^\top \Sigma \boldsymbol{\pi}_t)$. Hence, over this short interval,

$$X_{t+\Delta t} = X_t \exp\left([\beta - \alpha - \frac{1}{2} \boldsymbol{\pi}_t^\top \Sigma \boldsymbol{\pi}_t] \Delta t + \boldsymbol{\pi}_t^\top \mathbf{V} [\mathbf{W}_{t+\Delta t} - \mathbf{W}_t] \right).$$

When one iterates this stepwise update (e.g. in a Monte Carlo setting), it serves as a geometric or *exponential* Euler scheme. In special cases where $\boldsymbol{\pi}_t$ and α stay truly constant (e.g. infinite horizon with constant controls), a closed-form exponential solution for X_t then emerges over the entire horizon.

2.2 Objective Function and Neural Network Parametrization of Controls

We adopt a continuous-time utility-maximization objective analogous to the classical Merton setup:

$$J(\boldsymbol{\pi}_t, C_t) = \mathbb{E} \left[\int_0^T e^{-\rho t} U(C_t) dt + \kappa e^{-\rho T} U(X_T) \right], \quad (2)$$

where $\rho > 0$ is a continuous discount rate, $\kappa > 0$ is a bequest parameter, and U is a CRRA (constant relative risk aversion) utility:

$$U(x) = \frac{x^{1-\gamma}}{1-\gamma}, \quad \gamma > 0, \gamma \neq 1. \quad (3)$$

When $\gamma > 1$, the investor exhibits higher risk aversion, whereas $\gamma < 1$ corresponds to lower risk aversion, and $\gamma = 1$ (log utility) is often handled separately.

To solve this high-dimensional control problem, one typically parameterizes

$$\boldsymbol{\pi}_t = \boldsymbol{\pi}_\theta(t, X_t) \in \mathbb{R}^n, \quad C_t = C_\phi(t, X_t),$$

where θ, ϕ denote the neural-network parameters. The training objective is then $J(\theta, \phi) \approx J(\boldsymbol{\pi}_t, C_t)$, and one applies numerical methods to identify a locally (or globally) optimal policy.

2.3 Existence of Closed-Form Solutions in Special Cases

In the single-asset ($n = 1$) Merton problem with constant parameters and CRRA utility, one obtains well-known closed-form expressions for the *optimal portfolio proportion* π_t^* and the *optimal consumption rate* C_t^* . A notable extension is that these closed-form solutions also carry over to a *multi-asset* setting under similarly restrictive assumptions—namely, constant drift–volatility, infinite horizon, and no bequest ($\kappa = 0$). Consider first the infinite-horizon objective

$$\mathbb{E}\left[\int_0^\infty e^{-\rho t} U(C_t) dt\right],$$

where $\rho > 0$ is the discount rate, U is the CRRA utility (3), and $\kappa = 0$. Assume the drift vector $\boldsymbol{\mu}$, covariance matrix Σ , and risk-free rate r remain constant, and $\gamma \neq 1$. Under these conditions, the associated Hamilton–Jacobi–Bellman (HJB) equation yields a *time-invariant* optimal investment proportion $\boldsymbol{\pi}_t^*$ and a consumption rate C_t^* that is a constant fraction ν of wealth:

$$\boldsymbol{\pi}_t^* = \frac{1}{\gamma} \Sigma^{-1}(\boldsymbol{\mu} - r \mathbf{1}), \quad \forall t \geq 0, \quad (4)$$

$$C_t^* = \nu X_t \quad \text{with} \quad \nu = \frac{\rho - (1 - \gamma) \left(r + \frac{1}{2} (\boldsymbol{\mu} - r \mathbf{1})^\top \Sigma^{-1} (\boldsymbol{\mu} - r \mathbf{1}) \right)}{\gamma}. \quad (5)$$

Hence, even in multiple dimensions, the optimal portfolio weights remain *constant over time*, and consumption is *proportional* to current wealth.

When the horizon is finite $[0, T]$ or a bequest term $\kappa > 0$ is included, the optimal consumption rate C_t^* typically *depends explicitly on time*. In the single-asset finite-horizon case, one still obtains a known closed-form solution:

$$\pi_t^* = \frac{\mu - r}{\gamma \sigma^2}, \quad C_t^* = \alpha(t) X_t,$$

where

$$\alpha(t) = \left(\Phi(t) e^{-\rho t} \right)^{-\frac{1}{\gamma}}, \quad \Phi(t) = \exp\left\{ (T-t) \left[\rho(1-\gamma) - (1-\gamma)r - \frac{(\mu-r)^2}{2\gamma\sigma^2} \right] \right\}.$$

By analogy, in the multi-asset model with covariance matrix Σ , one replaces $(\mu - r)^2/\sigma^2$ by $(\boldsymbol{\mu} - r\mathbf{1})^\top \Sigma^{-1}(\boldsymbol{\mu} - r\mathbf{1})$, while retaining the same overall functional structure. Specifically,

$$\boldsymbol{\pi}_t^* = \frac{1}{\gamma} \Sigma^{-1}(\boldsymbol{\mu} - r\mathbf{1}), \quad C_t^* = \alpha(t) X_t,$$

for a suitably defined time-varying factor $\alpha(t)$. However, unlike the infinite-horizon case, $\alpha(t)$ is no longer constant and must be computed (for instance) via the finite-horizon HJB equation or an equivalent backward recursion.

Thus, while infinite-horizon, no-bequest settings admit elegant *constant-in-time* solutions (Equations (4)–(5)), more realistic problems with finite horizons, bequests, or time-varying parameters lose this closed-form tractability. The investor’s optimal consumption and allocation become time-dependent, and high-dimensional or correlated assets further complicate the HJB equation. These factors motivate the *numerical* and *deep learning* approaches explored in subsequent sections, such as our Pontryagin-Guided Direct Policy Optimization (PG-DPO) framework.

3 Pontryagin’s Principle for Multi-Asset Portfolio Problem

We now discuss how Pontryagin’s Maximum Principle (PMP) applies to the *multi-asset, continuous-time* Merton problem introduced in Section 2 (see also Pontryagin, 2018; Pardoux & Peng, 1990; Fleming & Soner, 2006; Pham, 2009 for further details on PMP). Although the *wealth* X_t itself is a single-dimensional state, the presence of multiple risky assets can introduce higher-dimensional controls $\boldsymbol{\pi}_t \in \mathbb{R}^n$. In particular, we focus on the *adjoint* (costate) processes arising from Pontryagin’s formulation and explore their relationship to both optimal and suboptimal (parameterized) policies in this multi-asset setting.

3.1 Pontryagin’s Maximum Principle for the Multi-Asset Merton Problem

Consider a multi-asset Merton model in which an investor allocates wealth X_t among n risky assets and consumes continuously over $[0, T]$. Let $\boldsymbol{\pi}_t \in \mathbb{R}^n$ be the

proportions of wealth invested in each of the n risky assets, and let C_t be the consumption rate. The wealth X_t then evolves according to

$$dX_t = \left[r X_t + X_t \boldsymbol{\pi}_t^\top (\boldsymbol{\mu} - r \mathbf{1}) - C_t \right] dt + X_t \boldsymbol{\pi}_t^\top \Sigma d\mathbf{W}_t, \quad X_0 = x_0 > 0,$$

where $r > 0$ is the risk-free rate, $\boldsymbol{\mu} \in \mathbb{R}^n$ is the vector of risky-asset drifts, $\Sigma \in \mathbb{R}^{n \times n}$ is a volatility matrix (assumed invertible in many cases), and $\mathbf{W}_t \in \mathbb{R}^n$ is an n -dimensional Brownian motion. The investor seeks to maximize

$$J(\boldsymbol{\pi}, C) = \mathbb{E} \left[\int_0^T e^{-\rho t} U(C_t) dt + \kappa e^{-\rho T} U(X_T) \right],$$

where $\rho > 0$ is a continuous discount rate, $\kappa > 0$ modulates the terminal wealth utility, and $U(x)$ is a concave utility function (e.g., CRRA).

To apply Pontryagin's Maximum Principle, define the Hamiltonian

$$\mathcal{H}(t, X_t, \boldsymbol{\pi}_t, C_t, \lambda_t, \mathbf{Z}_t) = e^{-\rho t} U(C_t) + \lambda_t \left[r X_t + X_t \boldsymbol{\pi}_t^\top (\boldsymbol{\mu} - r \mathbf{1}) - C_t \right] + \mathbf{Z}_t^\top \left(X_t \Sigma^\top \boldsymbol{\pi}_t \right), \quad (6)$$

where $\lambda_t \in \mathbb{R}$ is the scalar adjoint (costate) process for the one-dimensional state X_t , and $\mathbf{Z}_t \in \mathbb{R}^n$ is the costate associated with the multi-dimensional Brownian noise.

From a differential perspective, λ_t measures the *marginal effect* of changes in the current wealth X_t on the total expected utility J . In other words, $\lambda_t \approx \partial J / \partial X_t$. In classical HJB or PDE treatments, this corresponds to $\partial V / \partial x$ for a value function $V(t, x)$. Hence, a small increment in X_t can be evaluated by its influence on the overall objective, and λ_t encapsulates this sensitivity throughout the time horizon.

If $(\boldsymbol{\pi}_t^*, C_t^*)$ is optimal, the corresponding wealth X_t^* satisfies

$$dX_t^* = \left[r X_t^* + X_t^* (\boldsymbol{\pi}_t^*)^\top (\boldsymbol{\mu} - r \mathbf{1}) - C_t^* \right] dt + X_t^* (\boldsymbol{\pi}_t^*)^\top \Sigma d\mathbf{W}_t, \quad X_0^* = x_0,$$

while the pair $(\lambda_t^*, \mathbf{Z}_t^*)$ solves the backward SDE

$$d\lambda_t^* = - \frac{\partial \mathcal{H}}{\partial X} (t, X_t^*, \boldsymbol{\pi}_t^*, C_t^*, \lambda_t^*, \mathbf{Z}_t^*) dt + \mathbf{Z}_t^{*\top} d\mathbf{W}_t, \quad \lambda_T^* = \frac{\partial}{\partial X} \left[\kappa e^{-\rho T} U(X_T^*) \right].$$

Pontryagin's Maximum Principle states that $(\boldsymbol{\pi}_t^*, C_t^*)$ locally maximizes \mathcal{H} at each time t . Taking partial derivatives with respect to C_t and $\boldsymbol{\pi}_t$ and setting them to zero, one obtains

$$\frac{\partial \mathcal{H}}{\partial C_t} = e^{-\rho t} U'(C_t^*) - \lambda_t^* = 0, \quad \frac{\partial \mathcal{H}}{\partial \boldsymbol{\pi}_t} = \lambda_t^* X_t^* (\boldsymbol{\mu} - r \mathbf{1}) + X_t^* (\Sigma^\top \mathbf{Z}_t^*) = \mathbf{0}.$$

Specializing to CRRA utility $U(x) = \frac{x^{1-\gamma}}{1-\gamma}$ yields

$$C_t^* = \left(e^{\rho t} \lambda_t^* \right)^{-\frac{1}{\gamma}}, \quad \boldsymbol{\pi}_t^* = -\Sigma^{-1} \frac{\lambda_t^*}{X_t^*} \mathbf{Z}_t^*, \quad (7)$$

with $(\lambda_t^*, \mathbf{Z}_t^*)$ determined by the backward SDE. One often uses the identity

$$\mathbf{Z}_t^* = X_t^* \Sigma^\top \boldsymbol{\pi}_t^* (\partial_x \lambda_t^*),$$

where $\partial_x \lambda_t^* \equiv \frac{\partial}{\partial X} \lambda_t^*$. Substituting back into the first-order conditions can then provide explicit formulas for $\boldsymbol{\pi}_t^*$ in terms of λ_t^* and $\partial_x \lambda_t^*$.

In this manner, Pontryagin’s Maximum Principle transforms the continuous-time consumption–investment problem into a coupled forward–backward SDE in $(X_t^*, \lambda_t^*, \mathbf{Z}_t^*)$ combined with a pointwise maximization condition for $(\boldsymbol{\pi}_t^*, C_t^*)$. Crucially, these costate (adjoint) processes can be computed *automatically* within modern deep-learning frameworks such as PyTorch or JAX, simply by applying backpropagation to a stochastic rollout. Rather than solving high-dimensional PDEs or explicitly discretizing a backward SDE on a grid, one can sample forward paths, differentiate through them, and retrieve λ_t quickly. This insight forms the basis of our subsequent methods.

3.2 Policy-Fixed Adjoint Processes and Parameter Gradients

In a neural network setting, the policy $(\boldsymbol{\pi}_\theta, C_\phi)$ may be *suboptimal*, yet we can still define a *policy-fixed adjoint* by plugging $(\boldsymbol{\pi}_\theta, C_\phi)$ into the Hamiltonian \mathcal{H} (see (6)) and formulating the BSDE

$$\begin{aligned} d\lambda_t &= -\frac{\partial}{\partial X} \mathcal{H}\left(t, X_t, \boldsymbol{\pi}_\theta(t, X_t), C_\phi(t, X_t), \lambda_t, \mathbf{Z}_t\right) dt + \mathbf{Z}_t^\top d\mathbf{W}_t, \\ \lambda_T &= \frac{\partial}{\partial X} \left[\kappa e^{-\rho T} U(X_T) \right]. \end{aligned} \quad (8)$$

Here, λ_t and \mathbf{Z}_t capture local sensitivities of the suboptimal control with respect to changes in the state X_t . Although $\boldsymbol{\pi}_\theta$ and C_ϕ do not necessarily maximize \mathcal{H} , these adjoints remain well-defined under standard Lipschitz and integrability assumptions, thereby enabling a gradient-based improvement approach.

From a stochastic-calculus viewpoint (see Ma & Yong, 1999; Yong & Zhou, 2012), the gradient of the performance functional

$$J(\theta, \phi) = \mathbb{E} \left[\int_0^T e^{-\rho t} U(C_\phi(t, X_t)) dt + \kappa e^{-\rho T} U(X_T) \right]$$

with respect to policy parameters θ and ϕ can be written (symbolically) in a *Pontryagin-style* form:

$$\nabla_{\theta} J = \mathbb{E} \left[\int_0^T \left(\lambda_t \frac{\partial b}{\partial \theta} + \mathbf{Z}_t^{\top} \frac{\partial \sigma}{\partial \theta} \right) dt \right] + (\text{direct payoff derivative in } \theta), \quad (9)$$

$$\nabla_{\phi} J = \mathbb{E} \left[\int_0^T \left(\lambda_t \frac{\partial b}{\partial \phi} + \mathbf{Z}_t^{\top} \frac{\partial \sigma}{\partial \phi} \right) dt \right] + (\text{direct payoff derivative in } \phi). \quad (10)$$

Here, the terms $\lambda_t \frac{\partial b}{\partial \theta}$ and $\mathbf{Z}_t^{\top} \frac{\partial \sigma}{\partial \theta}$ capture how θ influences the *drift* and *diffusion* of X_t , while the *direct payoff derivative* accounts for any explicit dependence of $\int e^{-\rho t} U(C_{\phi}(t, X_t)) dt$ on θ . An analogous structure holds for ϕ .

In our portfolio optimization setting,

$$b(t, X, \boldsymbol{\pi}_{\theta}, C_{\phi}) = rX + X \boldsymbol{\pi}_{\theta}^{\top} (\boldsymbol{\mu} - r \mathbf{1}) - C_{\phi}, \quad \sigma(t, X, \boldsymbol{\pi}_{\theta}, C_{\phi}) = X \Sigma^{\top} \boldsymbol{\pi}_{\theta}.$$

Hence, we can compute

$$\frac{\partial b}{\partial \theta} = X (\boldsymbol{\mu} - r \mathbf{1})^{\top} \frac{\partial \boldsymbol{\pi}_{\theta}}{\partial \theta}, \quad \frac{\partial b}{\partial \phi} = -\frac{\partial C_{\phi}}{\partial \phi}, \quad \frac{\partial \sigma}{\partial \theta} = X \Sigma^{\top} \frac{\partial \boldsymbol{\pi}_{\theta}}{\partial \theta}, \quad \frac{\partial \sigma}{\partial \phi} = 0.$$

Meanwhile, the *direct* part of the payoff $\int_0^T e^{-\rho t} U(C_{\phi}(t, X_t)) dt$ contributes

$$\frac{\partial}{\partial \phi} [e^{-\rho t} U(C_{\phi}(t, X_t))] = e^{-\rho t} U'(C_{\phi}(\cdot)) \frac{\partial C_{\phi}(\cdot)}{\partial \phi}.$$

Putting these together, one obtains the expanded expressions:

$$\nabla_{\theta} J = \mathbb{E} \left[\int_0^T \left\{ \lambda_t X_t (\boldsymbol{\mu} - r \mathbf{1}) + X_t (\Sigma \mathbf{Z}_t) \right\}^{\top} \frac{\partial \boldsymbol{\pi}_{\theta}}{\partial \theta} dt \right], \quad (11)$$

$$\nabla_{\phi} J = \mathbb{E} \left[\int_0^T \lambda_t \left(-\frac{\partial C_{\phi}}{\partial \phi} \right) dt \right] + \mathbb{E} \left[\int_0^T e^{-\rho t} U'(C_{\phi}(\cdot)) \frac{\partial C_{\phi}(\cdot)}{\partial \phi} dt \right]. \quad (12)$$

Because $\frac{\partial \sigma}{\partial \phi} = 0$ under Merton's dynamics, $\mathbf{Z}_t^{\top} \frac{\partial \sigma}{\partial \phi}$ does not appear in $\nabla_{\phi} J$.

When $(\boldsymbol{\pi}_{\theta}, C_{\phi})$ eventually satisfies Pontryagin's conditions (i.e., it maximizes $\mathcal{H}(t, X_t, \boldsymbol{\pi}_t, C_t, \lambda_t, \mathbf{Z}_t)$ *pointwise*), the suboptimal adjoint $(\lambda_t, \mathbf{Z}_t)$ converges to the optimal adjoint $(\lambda_t^*, \mathbf{Z}_t^*)$. Hence, $\nabla_{\theta} J$ and $\nabla_{\phi} J$ vanish, and we recover $\boldsymbol{\pi}_t^*$ and C_t^* from the classical Pontryagin rule (cf. (7)). In effect, each gradient update moves $\boldsymbol{\pi}_{\theta}$ and C_{ϕ} closer to a Pontryagin-aligned solution in continuous time, iteratively refining investment and consumption rules until they resemble the well-known Merton policies.

This viewpoint also illustrates how backpropagation-based policy training serves as a *bridge* between modern deep learning and classical stochastic control: the adjoint process λ_t and its associated BSDE arise naturally from Pontryagin's principle, while automatic differentiation computes $\nabla_{\theta} J$ and $\nabla_{\phi} J$ in a single pass. Thus, despite the neural networks' high dimensionality, the underlying mathematical framework remains consistent with well-established control principles.

4 Gradient-Based Algorithm for Policy Optimization

Thus far, we have shown how Pontryagin’s Maximum Principle (PMP) yields a coupled forward-backward characterization of the optimal solution in the high-dimensional Merton problem. In practice, however, these continuous-time conditions must be approximated numerically. Here, we adopt a gradient-based scheme that leverages backpropagation through time (BPTT) to iteratively refine a neural-network policy. Our approach builds on the one-dimensional methods proposed by Huh (2024), who introduced the PG-DPO and PG-DPO-Align algorithms for the 1D Merton model, but we now extend these ideas to a full multi-asset setting and further propose a novel “OneShot” shortcut.

Concretely, we treat the adjoint processes λ_t, \mathbf{Z}_t as suboptimal costates under the current policy parameters, then update the policy to reduce the discrepancy between the induced Hamiltonian and its local Pontryagin maximum. To enhance training stability and accelerate convergence, we incorporate an alignment penalty (as in Huh, 2024) that encourages the learned policy (consumption and investment) to stay close to Pontryagin-derived controls. Additionally, we introduce a new “OneShot” procedure that directly extracts Pontryagin-aligned controls from the BPTT-derived adjoint, potentially bypassing the network’s outputs at inference time. Taken together, these techniques form a flexible family of Pontryagin-Guided Direct Policy Optimization (PG-DPO) methods, each offering different trade-offs in stability, convergence speed, and interpretability.

4.1 Single-Path Approach for Estimating Adjoint Processes

A key insight of our method is that one forward simulation (or single path) can produce an unbiased estimate of the adjoint processes λ_t and \mathbf{Z}_t at the visited time-state points (t_k, X_k) . Specifically, $\lambda_t = \frac{\partial J}{\partial X_t}$ captures how marginal variations in the scalar wealth process X_t affect the objective $J(\theta, \phi)$. In a *multi-asset* setting, $\mathbf{Z}_t \in \mathbb{R}^n$ similarly encodes how the noise directions in \mathbf{W}_t propagate through the policy’s diffusion terms. Once we differentiate the policy networks and the forward simulation via automatic differentiation, we can retrieve consistent estimates of λ_t and \mathbf{Z}_t by backpropagating from the scalar objective $J(\theta, \phi)$. Although the precise mapping between λ_t, \mathbf{Z}_t and the policy variables can differ across problem dimensions and parameterizations of Σ , the overarching idea remains: a single trajectory suffices to yield a pathwise (unbiased) estimate of the adjoint processes at each discrete (t_k, X_k) .

This single-path approach has several attractive properties. First, it is unbiased in the sense that, over many random draws, the average of the estimated adjoints

converges to the true costates in expectation (Kushner & Yin, 2003; Borkar & Borkar, 2008). Second, it is memory-efficient because each node (t_k, X_k) is visited by exactly one trajectory (or one mini-batch), avoiding the need to store large datasets or ensembles. Third, it is online-adaptive in that, as θ, ϕ are updated, new samples are drawn in real time, ensuring the policy remains well-trained for the state distribution induced by its latest parameters.

On the other hand, using only a single sample per node can lead to higher variance in gradient estimates, potentially slowing or destabilizing learning. In Section 4.3, we introduce an alignment penalty that can further reduce this variance and encourage smoother convergence, but one can also employ standard variance-reduction or larger mini-batch sampling if desired. Furthermore, Section 4.4 shows how we can leverage the adjoint estimates directly through a *OneShot* approach, bypassing the learned policy for faster inference if needed.

4.2 Discrete-Time Algorithm for Gradient Computation

We now detail a concrete procedure, in discrete time, for computing both the adjoint processes $(\lambda_t, \mathbf{Z}_t)$ and the parameter gradients $(\nabla_\theta J, \nabla_\phi J)$. This algorithm implements backpropagation-through-time (BPTT) for the *multi-asset* Merton problem, jointly handling consumption and multi-dimensional investment decisions. Concretely, the following steps outline the core of our PG-DPO approach in discrete time:

- (a) **Discretize Dynamics and Objective.** Partition the time interval $[0, T]$ into N steps of size $\Delta t = T/N$. Define $t_k = k \Delta t$ for $k = 0, \dots, N$, so that $t_0 = 0$ and $t_N = T$. We approximate the continuous-time SDE of (1) via an Euler–Maruyama scheme. At each step, with $\boldsymbol{\pi}_k = \boldsymbol{\pi}_\theta(t_k, X_k)$ and $C_k = C_\phi(t_k, X_k)$, we set

$$X_{k+1} = X_k + \left[r X_k + X_k \boldsymbol{\pi}_k^\top (\boldsymbol{\mu} - r \mathbf{1}) - C_k \right] \Delta t + X_k \boldsymbol{\pi}_k^\top \Sigma \Delta \mathbf{W}_k,$$

where $\Delta \mathbf{W}_k \sim \mathcal{N}(\mathbf{0}, \Delta t I_n)$. Meanwhile, the continuous-time objective

$$J(\theta, \phi) = \mathbb{E} \left[\int_0^T e^{-\rho t} U(C_t) dt + \kappa e^{-\rho T} U(X_T) \right] \quad (13)$$

is discretized as

$$J(\theta, \phi) \approx \mathbb{E} \left[\sum_{k=0}^{N-1} e^{-\rho t_k} U(C_k) \Delta t + \kappa e^{-\rho T} U(X_N) \right].$$

- (b) **Single Forward Path per** (t_k, X_k) . At each node (t_k, X_k) , we run exactly one forward simulation from k to the terminal index N . This yields a single-sample payoff, unbiased but subject to Monte Carlo variance. After the simulation, backpropagation (autodiff) yields local adjoint estimates λ_k and \mathbf{Z}_k under the current policy (θ, ϕ) .
- (c) **Compute** λ_k **via BPTT**. In typical deep-learning frameworks (e.g., PyTorch or JAX), we build a computational graph from (θ, ϕ) through $\{\boldsymbol{\pi}_k, C_k\}$ and $\{X_k\}$ to the approximate objective $J(\theta, \phi)$. A single call to `.backward()` (or equivalent) computes $\nabla_{\theta} J$ and $\nabla_{\phi} J$, as well as the partial derivatives of J with respect to each X_k . Identifying

$$\lambda_k = \frac{\partial J}{\partial X_k}$$

aligns with the Pontryagin perspective that λ_k is the (suboptimal) adjoint measuring the sensitivity of the overall cost to changes in X_k .

- (d) **Obtain** $\partial_x \lambda_k$ **and hence** \mathbf{Z}_k . To compute \mathbf{Z}_k , one typically needs $\partial_x \lambda_k$. In multi-asset Merton, a common approach differentiates the Hamiltonian or uses $\mathbf{Z}_k \approx [\partial_x \lambda_k] (X_k \Sigma^{\top} \boldsymbol{\pi}_k)$. Although this step does not *impose* optimality, it provides additional derivatives needed for constructing the exact parameter gradients (cf. (11)–(12)).
- (e) **Update Network Parameters**. Finally, we collect $\nabla_{\theta} J$ and $\nabla_{\phi} J$ and update (θ, ϕ) using a stochastic optimizer (e.g., Adam or SGD). In *discrete time*, one typically sums the integrands over $k = 0, \dots, N - 1$ with Δt . For example, the expanded $\nabla_{\theta} J$ might be approximated by

$$\nabla_{\theta} J \approx \mathbb{E} \left[\sum_{k=0}^{N-1} \left\{ \lambda_k X_k (\boldsymbol{\mu} - r \mathbf{1}) + X_k (\Sigma \mathbf{Z}_k) \right\}^{\top} \frac{\partial \boldsymbol{\pi}_{\theta}(t_k, X_k)}{\partial \theta} \Delta t \right], \quad (14)$$

while the expanded $\nabla_{\phi} J$ might be approximated by

$$\nabla_{\phi} J \approx \mathbb{E} \left[\sum_{k=0}^{N-1} \lambda_k \left(-\frac{\partial C_{\phi}(t_k, X_k)}{\partial \phi} \right) \Delta t \right] + \mathbb{E} \left[\sum_{k=0}^{N-1} e^{-\rho t_k} U'(C_k) \frac{\partial C_{\phi}(t_k, X_k)}{\partial \phi} \Delta t \right]. \quad (15)$$

By averaging these over M trajectories (or mini-batches), one obtains a stochastic approximation of $\nabla_{\theta} J$ and $\nabla_{\phi} J$. Repeating this process eventually yields a stationary policy.

In practice, one could simply define the neural policy $(\boldsymbol{\pi}_{\theta}, C_{\phi})$, compute $J(\theta, \phi)$ on simulated trajectories, and call `.backward()`; automatic differentiation then

handles the internal adjoint logic. Nonetheless, explicitly recognizing $(\lambda_k, \mathbf{Z}_k)$ as suboptimal Pontryagin adjoints clarifies why backpropagation works and how to incorporate additional alignment or constraints. Altogether, these steps form the foundation of our PG-DPO scheme in the multi-asset Merton setting.

4.3 Adjoint-Based Regularization for Pontryagin Alignment

Having shown how to compute online estimates of λ_k and \mathbf{Z}_k for extracting locally Pontryagin-optimal consumption and investment, we now introduce an alignment penalty that further steers the neural policy toward these ideal controls. When added to our baseline PG-DPO method (see Section 4.2), the resulting scheme becomes PG-DPO-Align.

In the multi-asset setting, the Pontryagin-based controls at each discrete node (t_k, X_k) generalize to

$$C^{\text{PMP}}(t_k, X_k) = \left(e^{\rho t_k} \lambda_k\right)^{-\frac{1}{\gamma}}, \quad \boldsymbol{\pi}^{\text{PMP}}(t_k, X_k) = -\Sigma^{-1} \frac{\lambda_k}{X_k} \mathbf{Z}_k, \quad (16)$$

mirroring (7) but evaluated with the suboptimal adjoint estimates $(\lambda_k, \mathbf{Z}_k)$. These formulas provide a local Pontryagin benchmark for consumption (C^{PMP}) and multi-asset investment ($\boldsymbol{\pi}^{\text{PMP}}$).

We define a soft penalty at each node (t_k, X_k) to encourage $(\boldsymbol{\pi}_\theta(t_k, X_k), C_\phi(t_k, X_k))$ to remain near $(\boldsymbol{\pi}^{\text{PMP}}(t_k, X_k), C^{\text{PMP}}(t_k, X_k))$. Concretely, let

$$\mathcal{L}_{\text{align}}(\theta, \phi) = \beta_C \sum_k \left\| C_\phi(t_k, X_k) - C^{\text{PMP}}(t_k, X_k) \right\| + \beta_\pi \sum_k \left\| \boldsymbol{\pi}_\theta(t_k, X_k) - \boldsymbol{\pi}^{\text{PMP}}(t_k, X_k) \right\|,$$

where $\|\cdot\|$ may be an absolute or squared norm, and $\beta_C, \beta_\pi > 0$ balance consumption versus investment alignment. We then augment the original objective $J(\theta, \phi)$ by defining

$$\tilde{J}(\theta, \phi) = J(\theta, \phi) - \mathcal{L}_{\text{align}}(\theta, \phi).$$

Maximizing \tilde{J} via gradient-based updates penalizes large deviations between the neural policies and the Pontryagin references, yielding the PG-DPO-Align variant.

Each gradient step pursues higher expected utility while reducing mismatch to Pontryagin’s local optimum. The coefficients β_C and β_π control how aggressively to enforce alignment. Moderate values gently guide the network toward $(C^{\text{PMP}}, \boldsymbol{\pi}^{\text{PMP}})$ without overpowering exploration or the baseline objective. Larger values enforce stricter adherence but can slow learning if the suboptimal adjoint estimates are initially unreliable. We adopt a soft penalty to nudge the policy in the desired direction rather than imposing a hard constraint. Together with the baseline PG-DPO algorithm, this alignment penalty defines the PG-DPO-Align method, which can significantly improve stability and convergence speed in multi-asset Merton experiments.

4.4 PG-DPO-OneShot: A Modular Shortcut from BPTT-Derived Adjoint

We now describe a modular “OneShot” add-on, which leverages the fact that the adjoint (costate) process λ_t can converge rapidly under backpropagation-through-time (BPTT), even if the policy networks (π_θ, C_ϕ) remain suboptimal. By treating $\lambda_t \approx \frac{\partial J}{\partial X_t}$ as a gateway to Pontryagin’s principle, one can generate near-optimal controls without strictly relying on the networks at test time. In essence, OneShot acts as a “shortcut” that transforms the suboptimal adjoint into analytically derived decisions, thereby bypassing potentially slow or locally trapped network training.

Concretely, after simulating a batch of trajectories and computing $\lambda_k = \frac{\partial J}{\partial X_k}$ (and \mathbf{Z}_k , if needed) at each node (t_k, X_k) , one substitutes these into Pontryagin’s condition. For instance, in a multi-asset Merton model with a covariance matrix $\Sigma \in \mathbb{R}^{n \times n}$, one might compute π^{PMP} and C^{PMP} using (16). At test time, one can simply ignore the learned π_θ and C_ϕ , deploying $(\pi_k^{\text{PMP}}, C_k^{\text{PMP}})$ directly for near-optimal investment and consumption. This procedure effectively turns λ_t into a function-like control generator, requiring only a small computational overhead whenever a new (t_0, x_0) is encountered.

In practice, OneShot can be combined with either the baseline PG-DPO or the alignment-penalty version PG-DPO-Align. One first runs a partial training phase to stabilize λ_t , regardless of whether an alignment penalty is in use. If alignment is turned off, one obtains a variant that we may call PG-DPO-OneShot, where the final controls at test time come from Pontryagin formulas rather than the neural policies. If alignment is turned on, one obtains PG-DPO-Align-OneShot, where the policy is both nudged toward Pontryagin’s solution during training and then ignored at test time in favor of the directly computed Pontryagin controls. Either way, the user retains the option to deploy the networks themselves if desired, but by default, OneShot discards the policy outputs once the costate λ_t becomes accurate.

Although OneShot does not produce a final policy network for direct deployment, it remains highly flexible. In on-demand scenarios, one can simply run a brief forward simulation and backprop for each new initial state, using the costate-based route to generate near-optimal controls without further network training. This approach complements the alignment-penalty strategy in Section 4.3; both leverage the adjoint λ_t , but OneShot discards the policy network at test time, while alignment directly incorporates Pontryagin constraints into training. Numerical experiments (Section 5) confirm that OneShot can substantially reduce the training burden, achieving near-optimal performance even with a moderate warm-up phase, whether or not the alignment penalty is employed.

4.5 Extended Value Function and Algorithmic Variants

4.5.1 Extended Value Function and Discretized Rollouts

In Section 4.2, we introduced a discretization scheme for the Merton problem over a fixed interval $[0, T]$. Here, we extend that approach to handle any initial time t_0 and wealth x_0 by defining an extended value function over a broader domain.

Many continuous-time problems (including Merton) require a policy $(\boldsymbol{\pi}_\theta, C_\phi)$ valid for any initial condition (t_0, x_0) . To address this requirement, we define an *extended value function* that integrates over random initial nodes $(t_0, x_0) \sim \eta(\cdot)$ in the domain $\mathcal{D} \subset [0, T] \times (0, \infty)$, and then discretize each resulting trajectory. Here, η denotes the distribution of (t_0, x_0) . Concretely, we set

$$\widehat{J}(\theta, \phi) = \mathbb{E}_{(t_0, x_0) \sim \eta} \left[\mathbb{E} \left(\int_{t_0}^T e^{-\rho u} U(C_\phi(u, X_u)) du + \kappa e^{-\rho T} U(X_T) \right) \right].$$

Hence, maximizing $\widehat{J}(\theta, \phi)$ yields a policy $(\boldsymbol{\pi}_\theta, C_\phi)$ that applies across all sub-intervals $[t_0, T]$ and initial wealth x_0 .

To avoid overfitting to a single initial scenario, we draw (t_0, x_0) from a suitable distribution η . By doing so, the policy $(\boldsymbol{\pi}_\theta, C_\phi)$ is trained to cover a broad region of the time–wealth domain rather than just one initial condition. This sampling strategy is standard in many PDE-based or RL-like continuous-time methods that need a single control law $(\boldsymbol{\pi}_\theta, C_\phi)$ covering all (t, x) .

To implement the integral in $\widehat{J}(\theta, \phi)$, one can follow the step-by-step procedure in Algorithm 1, which details how to discretize the interval, simulate each path, and apply backpropagation to update (θ, ϕ) .

4.5.2 Gradient-Based Algorithmic Variants

Having introduced the extended value function $\widehat{J}(\theta, \phi)$ over random initial nodes (t_0, x_0) , we now present four PG-DPO methods for the multi-asset Merton problem. All four rely on the same procedure of simulating from sampled initial conditions and computing a stochastic estimate of $\widehat{J}(\theta, \phi)$. They differ in whether an *alignment penalty* is included, and whether one *deploys the learned networks* or a *one-shot Pontryagin control* at test time.

(a) PG-DPO (No Alignment, No One-Shot).

This is the *baseline* scheme, described in Algorithm 1. It optimizes \widehat{J} directly via backpropagation-through-time (BPTT), with no alignment penalty and no special one-shot step. Empirically, PG-DPO converges reliably toward Pontryagin-aligned solutions, albeit with potentially slower or noisier training in higher-dimensional (portfolio) contexts.

Algorithm 1 PG-DPO (No Alignment Penalty)

Inputs:

- Policy nets (π_θ, C_ϕ)
- Step sizes $\{\alpha_k\}$, total iterations K
- Domain sampler η for $(t_0^{(i)}, x_0^{(i)})$ over $\mathcal{D} \subset [0, T] \times (0, \infty)$
- Fixed integer N (number of time steps per path)

1: **for** $j = 1$ to K **do**

2: **(a) Sample mini-batch of size M :** For each $i \in \{1, \dots, M\}$, draw $(t_0^{(i)}, x_0^{(i)}) \sim \eta$.

3: **(b) Local Single-Path Simulation for each i :**

(a) *Define local step:* $\Delta t^{(i)} \leftarrow \frac{T-t_0^{(i)}}{N}$, $t_0^{(i)} < t_1^{(i)} < \dots < t_N^{(i)} = T$, where $t_k^{(i)} = t_0^{(i)} + k \Delta t^{(i)}$.

(b) *Initialize wealth:* $X_0^{(i)} \leftarrow x_0^{(i)}$.

(c) *Euler–Maruyama:* For $k = 0, \dots, N - 1$:

$$X_{k+1}^{(i)} = X_k^{(i)} + \left[r X_k^{(i)} + X_k^{(i)} \pi_\theta(t_k^{(i)}, X_k^{(i)})^\top (\boldsymbol{\mu} - r \mathbf{1}) - C_\phi(t_k^{(i)}, X_k^{(i)}) \right] \Delta t^{(i)} \\ + X_k^{(i)} \pi_\theta(t_k^{(i)}, X_k^{(i)})^\top \Sigma \Delta \mathbf{W}_k^{(i)},$$

where $\Delta \mathbf{W}_k^{(i)} \sim \mathcal{N}(\mathbf{0}, \Delta t^{(i)} I_n)$.

(d) *Local cost:*

$$J^{(i)}(\theta, \phi) = \sum_{k=0}^{N-1} e^{-\rho t_k^{(i)}} U\left(C_\phi(t_k^{(i)}, X_k^{(i)})\right) \Delta t^{(i)} + \kappa e^{-\rho T} U(X_N^{(i)}).$$

4: **(c) Backprop (single pass) & Averaging:**

$$\widehat{J}(\theta, \phi) = \frac{1}{M} \sum_{i=1}^M J^{(i)}(\theta, \phi), \quad \nabla_{(\theta, \phi)} \widehat{J} \leftarrow \text{BPTT on each } J^{(i)}.$$

5: **(d) Parameter Update:**

$$\theta \leftarrow \theta + \alpha_k \nabla_\theta \widehat{J}, \quad \phi \leftarrow \phi + \alpha_k \nabla_\phi \widehat{J}.$$

6: **end for**

7: **return** Final policy (π_θ, C_ϕ) .

Algorithm 2 PG-DPO-Align (With Alignment Penalty)

Additional Inputs:

- Alignment weights (β_C, β_π) ;
- Suboptimal adjoint $(\lambda_0^{(i)}, \frac{\partial}{\partial x} \lambda_0^{(i)})$ from an extra autodiff pass.

1: **for** $j = 1$ to K **do**

2: **(a) Domain Sampling & Single-Path Simulation:** *Same as PG-DPO.*
Collect each local cost $J^{(i)}(\theta, \phi)$.

3: **(b) Retrieve Adjoint Info (2nd pass):**

 i) For each path i , run an extra autodiff to obtain

$$\lambda_0^{(i)} = \frac{\partial J^{(i)}}{\partial X_0^{(i)}}, \quad \frac{\partial}{\partial x} \lambda_0^{(i)}.$$

 ii) Next, compute

$$\mathbf{Z}_0^{(i)} = \left[\frac{\partial}{\partial x} \lambda_0^{(i)} \right] \left(X_0^{(i)} \Sigma^\top \boldsymbol{\pi}_\theta(t_0^{(i)}, X_0^{(i)}) \right).$$

 iii) Finally, use these to obtain $\boldsymbol{\pi}_0^{\text{PMP},(i)}$ and $C_0^{\text{PMP},(i)}$.

$$C_0^{\text{PMP},(i)} = \left(e^{\rho t_0^{(i)}} \lambda_0^{(i)} \right)^{-\frac{1}{\gamma}}, \quad \boldsymbol{\pi}_0^{\text{PMP},(i)} = -\Sigma^{-1} \frac{\lambda_0^{(i)}}{X_0^{(i)}} \mathbf{Z}_0^{(i)}.$$

4: **(c) Full Objective with Alignment Penalty:**

$$\begin{aligned} \widehat{J}_{\text{align}}(\theta, \phi) = \frac{1}{M} \sum_{i=1}^M & \left[J^{(i)}(\theta, \phi) - \beta_C \|C_\phi(t_0^{(i)}, X_0^{(i)}) - C_0^{\text{PMP},(i)}\| \right. \\ & \left. - \beta_\pi \|\boldsymbol{\pi}_\theta(t_0^{(i)}, X_0^{(i)}) - \boldsymbol{\pi}_0^{\text{PMP},(i)}\| \right]. \end{aligned}$$

5: **(d) BPTT & Update:**

$$\nabla_\theta \widehat{J}_{\text{align}}, \nabla_\phi \widehat{J}_{\text{align}} \leftarrow \text{BPTT on each term.}$$

$$\theta \leftarrow \theta + \alpha_k \nabla_\theta \widehat{J}_{\text{align}}, \quad \phi \leftarrow \phi + \alpha_k \nabla_\phi \widehat{J}_{\text{align}}.$$

6: **end for**

7: **return** Final policy $(\boldsymbol{\pi}_\theta, C_\phi)$ balancing \widehat{J} and the alignment penalty.

Algorithm 3 PG-DPO-OneShot (Direct Pontryagin Controls)

Additional Inputs:

- A brief “warm-up” training phase (e.g., K_0 iterations of PG-DPO).
- Suboptimal adjoint λ_k and its derivative $\frac{\partial}{\partial x}\lambda_k$, from BPTT.

1: **(a) Partial Training:**

- (a) Run PG-DPO for a small number of iterations K_0 . Although the networks π_θ, C_ϕ may be suboptimal, the costate $\lambda_t \approx \frac{\partial J}{\partial X_t}$ often converges quickly.
- (b) After this warm-up, retrieve λ_0 (and $\frac{\partial}{\partial x}\lambda_0$) at the initial node (t_0, X_0) .

2: **(b) Compute \mathbf{Z}_0 :**

$$\mathbf{Z}_0 = \left[\frac{\partial}{\partial x}\lambda_0 \right] \left(X_0 \Sigma^\top \pi_\theta(t_0, X_0) \right).$$

3: **(c) OneShot Pontryagin Controls:**

$$C_0^{\text{PMP}} = \left(e^{\rho t_0} \lambda_0 \right)^{-\frac{1}{\gamma}}, \quad \pi_0^{\text{PMP}} = -\Sigma^{-1} \frac{\lambda_0}{X_0} \mathbf{Z}_0.$$

At test time, *ignore* the outputs of π_θ and C_ϕ , deploying $(\pi_0^{\text{PMP}}, C_0^{\text{PMP}})$ directly.

4: **return** *OneShot policy* $(\pi_0^{\text{PMP}}, C_0^{\text{PMP}})$ derived from the suboptimal adjoint.

(b) PG-DPO-Align (Alignment Penalty, No One-Shot).

This method extends the baseline by adding an alignment penalty $\mathcal{L}_{\text{align}}$ that nudges (π_θ, C_ϕ) closer to Pontryagin-derived controls at each iteration. As shown in Algorithm 2, we perform a second autodiff pass to retrieve $\lambda_0 \approx \frac{\partial J}{\partial X_0}$ (and its derivative) at the initial node, then penalize any deviation between $(\pi_\theta(t_0), C_\phi(t_0))$ and $(\pi_0^{\text{PMP}}, C_0^{\text{PMP}})$. Although this extra pass adds computation, it often accelerates or stabilizes convergence, preventing the learned policy from drifting far from Pontryagin conditions.

(c) PG-DPO-OneShot (No Alignment, One-Shot).

A third variant leverages the fact that the costate λ_t (adjoint) may converge faster than the policy networks themselves. After a brief warm-up phase of standard PG-DPO, we extract $\lambda_k \approx \frac{\partial J}{\partial X_k}$ and \mathbf{Z}_k from BPTT, then compute $(\pi_k^{\text{PMP}}, C_k^{\text{PMP}})$ via the Pontryagin formula (see Algorithm 3). At test time,

we *ignore* the neural-network outputs and directly deploy those one-shot Pontryagin controls. This can greatly reduce training requirements, although it foregoes having an explicit policy network for production use.

(d) **PG-DPO-Align-OneShot (Alignment Penalty + One-Shot).**

Finally, one may *combine* alignment and one-shot in a single framework. In this scenario, (π_θ, C_ϕ) is guided toward Pontryagin conditions during training via $\mathcal{L}_{\text{align}}$, while the *actual* decisions at test time still come from the one-shot Pontryagin formula. This two-layer approach can further stabilize the costate estimation and ensure near-optimal decisions, though it requires additional overhead for both alignment and final one-shot steps.

All four methods *extend naturally to the multi-asset case* by relying on the Pontryagin formulas in (16). One typically draws (t_0, x_0) from a chosen distribution η , ensuring coverage of various times and wealth levels. In practice, only λ_0 (and $\frac{\partial}{\partial x}\lambda_0$) need to be computed at the initial node if we use alignment or one-shot; higher-index states $\{X_k\}_{k=1}^N$ are handled by standard backprop. This framework is thus flexible: one can *mix* and match *Align* and *OneShot* to yield the four variants above, tailoring training overhead and deployment strategy to the user’s preferences and requirements.

For completeness, a detailed proof of convergence for a *single-asset* setting can be found in Huh (2024), including a rigorous analysis of how the neural policy and the Pontryagin adjoint interact to drive the gradient updates. Although that analysis is restricted to one-dimensional wealth processes, it carries over naturally to multi-asset problems under mild technical assumptions (e.g., sufficient differentiability of the policy nets and Lipschitz continuity in the drift and diffusion terms).

5 Numerical Results

In this section, we illustrate how our Pontryagin-guided framework applies to a *multi-asset* Merton problem that integrates both portfolio allocation and continuous consumption. While many recent *deep learning* methods for stochastic control—including deep BSDE approaches (e.g., Han et al., 2018; Weinan, 2017), PINNs (Raissi et al., 2019), and model-free RL (e.g., Reppen et al., 2023; Reppen & Soner, 2023; Dai et al., 2023)—often focus on single-asset or simpler PDE settings, we here address both *multi-asset investment* and *consumption* in a unified continuous-time framework. Moreover, traditional dynamic programming methods (e.g., Campbell & Viceira, 1999; Lynch & Balduzzi, 2000; Brandt et al., 2005) typically fail to scale beyond six or so risky assets due to the curse of dimension-

ality. By contrast, our approach remains tractable even for portfolios with up to 1,000 risky assets.

We evaluate our baseline **PG-DPO** algorithm alongside three extensions. First, **PG-DPO-Align** adds an adjoint-based alignment penalty. Second, **PG-DPO-OneShot** directly extracts Pontryagin controls from the learned adjoint (bypassing the neural networks at test time). Third, **PG-DPO-Align-OneShot** combines both alignment and direct Pontryagin extraction in a single framework. Our experiments span various problem sizes, culminating in scenarios with up to 10,000 risky assets, thereby demonstrating the feasibility of large-scale continuous-time portfolio optimization within a unified neural framework.

5.1 Experimental Setup

We consider horizons up to $T = 1$ and confine the wealth domain to $[0.1, 2]$. For each multi-asset scenario, the number of risky assets (denoted by n) can take values in $\{10, 100, 1000, 10000\}$. To obtain a stable yet varied set of market parameters (μ, Σ) , we adopt a random-correlation-based procedure:

- (a) **Correlation and Volatility.** We first generate a positive-definite correlation matrix $\mathbf{C} \in \mathbb{R}^{n \times n}$ (ensuring unit diagonal) and draw each asset’s volatility σ_i from $[\nu_{\min}, \nu_{\max}] = [0.05, 0.5]$. We then form the covariance matrix Σ by

$$\Sigma = \text{diag}(\boldsymbol{\sigma}) \mathbf{C} \text{diag}(\boldsymbol{\sigma}),$$

thereby controlling both volatility and correlation in a realistic range.

- (b) **Baseline Portfolio Constraints.** We generate an initial portfolio $\pi = (\pi_1, \dots, \pi_n) \in \mathbb{R}^n$ by sampling each component π_i from $[\pi_{\min}, \pi_{\max}]$, where $\pi_{\min} = -1.0$ and $\pi_{\max} = 2.0$. Let

$$s = \sum_{i=1}^n \pi_i.$$

If s lies outside a target interval $[s_{\min}, s_{\max}]$ (for example $[0.2, 0.75]$), we rescale π so that its new sum remains within $[s_{\min}, s_{\max}]$. Concretely,

$$\pi \leftarrow \pi \times \frac{\alpha}{s}, \quad \text{where } \alpha = \begin{cases} s_{\min}, & \text{if } s < s_{\min}, \\ s_{\max}, & \text{if } s > s_{\max}. \end{cases}$$

This prevents degenerate portfolios, e.g. those with overly high leverage $\sum_i \pi_i \gg 1$ or near-zero exposure $\sum_i \pi_i \approx 0$.

(c) **Drift Vector.** Finally, each asset’s drift μ_i is defined by

$$\mu_i = r + \gamma \sum_{j=1}^n \Sigma_{i,j} \pi_j, \quad i = 1, \dots, n,$$

where $r = 0.03$ is the risk-free rate and $\gamma = 2.0$ is a risk-aversion parameter. For the large-scale case ($n = 1000$), we fix a random seed (e.g., 42) to ensure reproducibility. This setup keeps Σ in a moderate range while preventing the baseline portfolio π from becoming extreme or trivial.

In addition, we set a discount rate $\rho = 0.1$ in the objective and choose $\varepsilon = 0.1$ for any noise scaling (when applicable). We allow up to $m = 5$ simulation steps per rollout. As mentioned before, the maximum time horizon is $T_{\max} = 1$, with wealth restricted to $[0.1, 2]$. Typically, we sample 10^3 initial states (t_0, X_0) at each training iteration, drawing each pair uniformly from $[0, T_{\max}] \times [0.1, 2]$. For each sampled initial pair, we set the local time step $\Delta t = (T_{\max} - t_0)/m$ and perform Euler–Maruyama updates to simulate forward to time T_{\max} .

We define two neural networks, $(C_\phi, \boldsymbol{\pi}_\theta)$, to parameterize the *consumption* and *investment* strategies, respectively. Both networks have two hidden layers (200 nodes each) with Leaky-ReLU activation. For the *consumption* network C_ϕ , we include a softplus activation in the final layer to ensure outputs remain strictly nonnegative.

We train these networks for 100,000 gradient steps using the Adam optimizer. For problems with up to $n = 1,000$ assets, we typically use a learning rate of 10^{-5} . However, at $n = 10,000$, this rate occasionally causes instabilities in training; thus we reduce it to 10^{-6} for the $n = 10,000$ case. After simulating forward with the current policy parameters, we compute the resulting payoff and apply backpropagation-through-time (BPTT) to update ϕ and θ . By dynamically re-drawing initial states (t_0, X_0) at each iteration, we avoid overfitting to any single dataset and gradually cover the time–wealth domain $[0, T] \times [0.1, 2]$.

5.2 Results for Multi-Asset Cases

We compare four PG-DPO variants in multi-asset settings with $n \in \{10, 100, 1000, 10000\}$: (i) *PG-DPO*, (ii) *PG-DPO-Align (AL)*, (iii) *PG-DPO-OneShot (OS)*, and (iv) *PG-DPO-Align-OneShot (AL-OS)*. This extends the single-asset study in Huh (2024), where PG-DPO alone was sufficient for fast, stable convergence. By contrast, once the number of risky assets grows, we observe that the baseline PG-DPO can become slow or inaccurate when learning the optimal investment policy. Even for as few as ten assets, PG-DPO’s convergence speed often remains too slow for practical use, and for $n = 100$ or $n = 1000$ assets, the baseline method can yield

alarmingly large relative errors (e.g., on the order of 100%–1000% for many assets). With $n = 10,000$, the table indicates that PG-DPO’s investment MSE can still be in the hundreds or thousands, corresponding to tens or hundreds of thousands of percentage points of error for some assets.

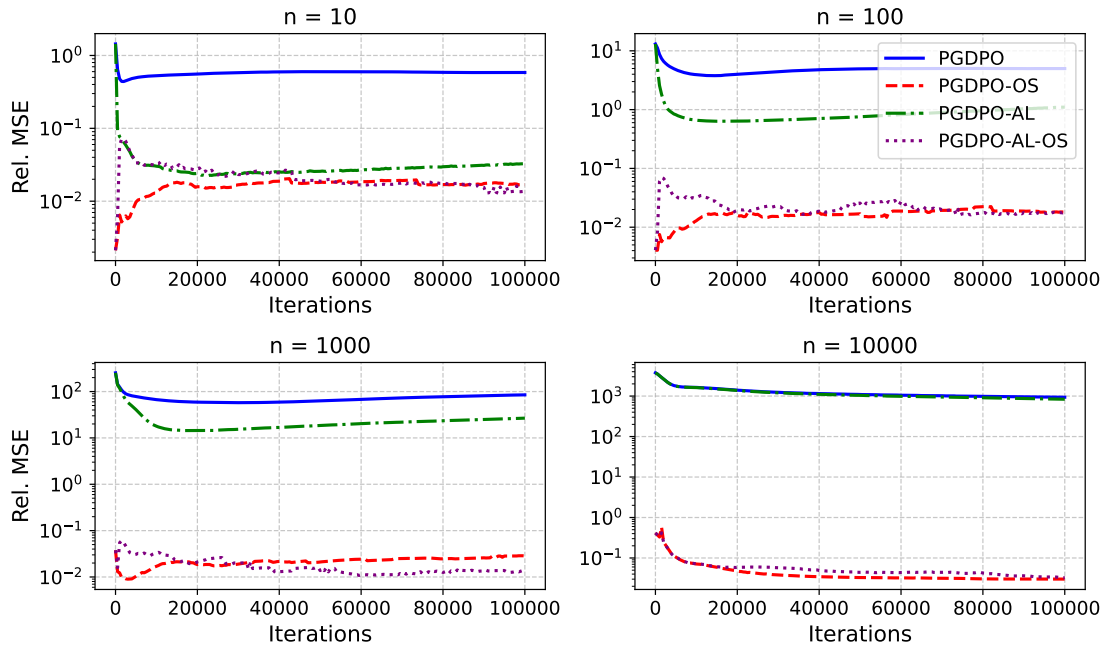
Table 1 provides a more quantitative perspective on the final (relative MSE) numbers for each method under different asset dimensions ($n = 10, 100, 1000, 10000$) and at different iteration milestones (1,000, 10,000, 100,000). The left block in the table shows the consumption errors (compared against the infinite-horizon benchmark), while the right block shows the investment errors (compared against the multi-asset Merton solution). The results confirm that PG-DPO alone has difficulty keeping error levels down in higher dimensions, whereas OS-based methods consistently produce much smaller relative MSE across all settings.

Table 1: Summary of relative MSE (lower is better) for consumption and investment under various PG-DPO methods, measured at three iteration milestones (1k, 10k, 100k). Space is also reserved for the case of 10k assets ($n = 10000$).

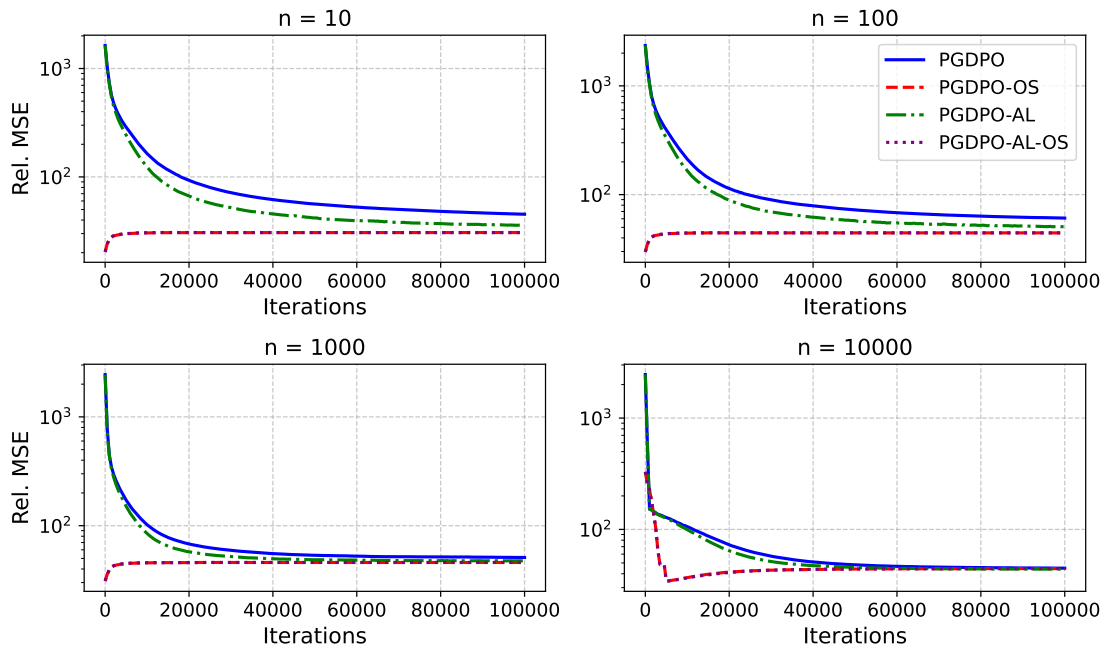
Assets	Method	Consumption (MSE)			Investment (MSE)		
		1k	10k	100k	1k	10k	100k
10	PG-DPO	7.34e+02	1.64e+02	4.53e+01	4.77e-01	5.30e-01	5.84e-01
	PG-DPO-AL	7.16e+02	1.23e+02	3.59e+01	7.67e-02	3.02e-02	3.28e-02
	PG-DPO-OS	2.66e+01	3.04e+01	3.07e+01	6.46e-03	1.29e-02	1.69e-02
	PG-DPO-AL-OS	2.63e+01	3.06e+01	3.06e+01	5.83e-02	3.27e-02	1.37e-02
100	PG-DPO	1.05e+03	2.12e+02	6.09e+01	8.70e+00	3.93e+00	4.99e+00
	PG-DPO-AL	1.02e+03	1.65e+02	5.08e+01	2.57e+00	6.60e-01	1.10e+00
	PG-DPO-OS	3.87e+01	4.43e+01	4.45e+01	7.53e-03	1.29e-02	1.81e-02
	PG-DPO-AL-OS	3.83e+01	4.45e+01	4.45e+01	6.02e-02	3.29e-02	1.82e-02
1000	PG-DPO	4.45e+02	1.02e+02	5.10e+01	1.25e+02	6.69e+01	8.49e+01
	PG-DPO-AL	4.38e+02	8.47e+01	4.75e+01	1.18e+02	1.79e+01	2.67e+01
	PG-DPO-OS	3.94e+01	4.56e+01	4.59e+01	1.23e-02	1.70e-02	2.84e-02
	PG-DPO-AL-OS	3.91e+01	4.57e+01	4.59e+01	5.48e-02	3.28e-02	1.34e-02
10000	PG-DPO	1.52e+02	1.06e+02	4.49e+01	3.20e+03	1.64e+03	9.36e+02
	PG-DPO-AL	1.52e+02	9.93e+01	4.40e+01	3.20e+03	1.62e+03	8.35e+02
	PG-DPO-OS	2.26e+02	3.69e+01	4.45e+01	3.29e-01	7.10e-02	3.00e-02
	PG-DPO-AL-OS	2.30e+02	3.67e+01	4.45e+01	3.29e-01	7.11e-02	3.25e-02

Figures 1a and 1b further illustrate how these difficulties arise when we plot the mean-squared errors (MSE) of investment and consumption relative to each respective reference. For the *investment* network, the closed-form multi-asset Merton solution provides a direct comparison, while for the *consumption* network we rely on the infinite-horizon Merton formula as a proxy for finite-horizon truth.

When adding *alignment* (PG-DPO-Align), we generally observe more stable training than with PG-DPO alone, especially as the number of assets increases. In the single-asset context studied by Huh (2024), the benefit of alignment was



(a) Investment MSE.



(b) Consumption MSE.

Figure 1: Relative MSE results over 100k iterations. Panel (a) shows the *investment* policy MSE, while panel (b) shows the *consumption* policy MSE.

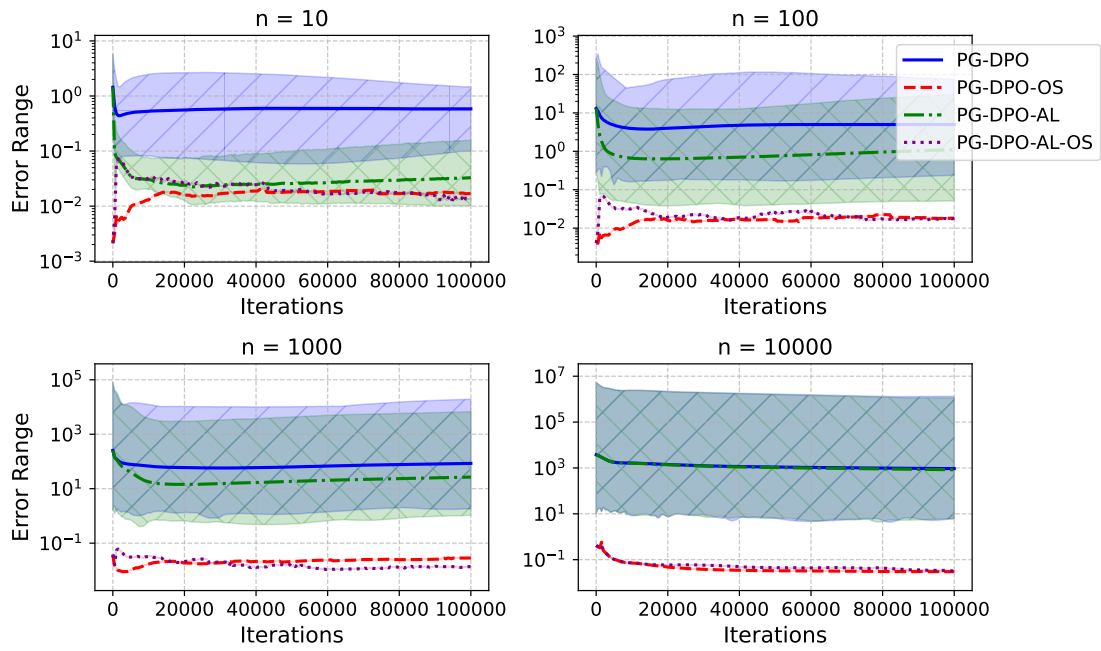


Figure 2: Min-max ranges of *investment* MSE across assets at each iteration.

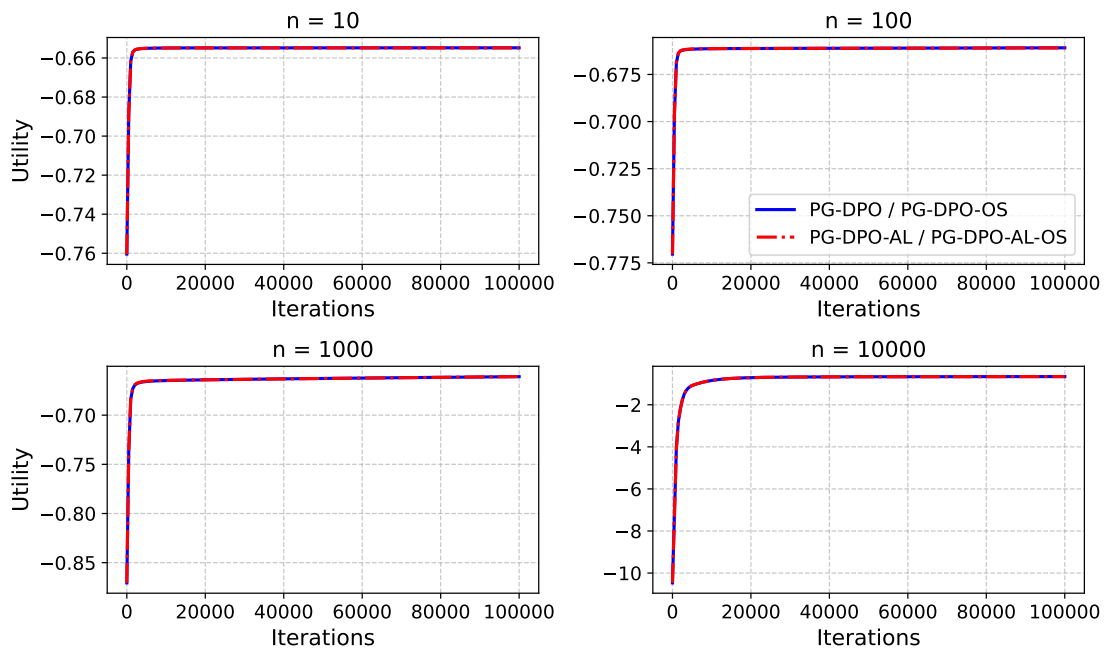


Figure 3: Empirical utility evolution (rolling 500-iteration averages).

marginal, but for multi-asset problems with $n > 10$ it becomes much more pronounced. Even so, alignment alone can still be slow to reduce the relative MSE when the portfolio dimension is extremely large.

By contrast, introducing the *one-shot* approach (PG-DPO-OneShot) yields much faster convergence, regardless of the number of assets. Even within a few thousand iterations, PG-DPO-OS can reduce the relative investment MSE below 10% in most cases. Notably, on an RTX 4090 GPU, 100,000 iterations take about one hour, so only a few thousand iterations often require just one or two minutes. Thus, for OS-based methods, it is feasible to achieve near-accurate solutions within a tiny fraction of the overall training budget, making OS immediately practical at virtually any scale. A key advantage is that OS enforces the *same* relative error across all assets, whereas non-OS methods often produce highly variable accuracy for different assets (e.g., some with hundreds or thousands of percent error while others are much lower). Directly applying Pontryagin’s formula from a single scalar adjoint λ ensures consistency across assets and gives a significant speedup in convergence.

Lastly, we examine the combined approach, PG-DPO-Align-OneShot. Early on, AL-OS may underperform OS alone, but over more iterations, the alignment term effectively drives the investment network to a better local minimum, thus improving the subsequent one-shot step. Hence, AL-OS typically surpasses OS in the long run. Intuitively, alignment offers additional guidance to the underlying policy network, rather than relying solely on the Pontryagin-adjoint shortcut at inference.

Figures 2 and 3 provide further detail on per-asset performance and overall utility evolution. In Figure 2, the min–max shaded band of relative investment MSE across all assets is quite broad for PG-DPO and PG-DPO-AL, indicating that many assets can have large errors while others remain small. By contrast, OS-based methods do not merely narrow the band—they collapse its width to zero because a single scalar adjoint enforces the same relative MSE for every asset once one-shot controls are applied.

Figure 3 shows that all methods improve utility over time, eventually converging to similar values. However, the objective function J is not always sensitive enough to detect whether policies are truly near-optimal or only moderately so, possibly due to flat directions in the objective landscape. Without additional Pontryagin guidance, policy gradients can converge to wide plateaus that fail to yield highly accurate investments across all assets.

In conclusion, while PG-DPO alone sufficed for single-asset problems (Huh, 2024), it struggles under multi-asset settings unless the portfolio dimension is small. PG-DPO-Align helps when the number of assets is moderate but can remain slow at very large scales. On the other hand, PG-DPO-OneShot routinely

achieves fast, uniform error reductions across dimensions and requires only minimal computation time (often just one or two minutes for a few thousand iterations), making it highly practical. PG-DPO-Align-OneShot merges both ideas and generally outperforms OS alone when sufficient training time is available, thanks to alignment guiding the network to a better region. The same overall patterns appear in consumption, although precise numerical comparisons are more challenging there in the absence of a true finite-horizon reference. Nonetheless, the consistency and variance-reduction benefits of OS, along with the gradual improvement from alignment, carry over qualitatively to the consumption network as well.

6 Conclusion

We have presented a Pontryagin-Guided Direct Policy Optimization (PG-DPO) framework that solves large-scale multi-asset Merton problems without relying on intractable dynamic programming grids. By weaving Pontryagin’s Maximum Principle (PMP) into a continuous-time neural-network parameterization, the method ensures that each gradient update follows locally optimal controls in expectation. Our experiments demonstrate that PG-DPO scales to portfolios with up to 10,000 risky assets, substantially extending earlier works that handled far fewer assets. Notably, in practice, even 100,000 gradient steps (enough to achieve very high accuracy) often complete in under an hour on a modern GPU, and just 1–2 minutes of training (a few thousand iterations) can already yield near-optimal solutions at virtually any dimension.

The numerical tests reveal several key takeaways. First, while the baseline PG-DPO performs reliably even at high dimensions, it can converge rather slowly if the number of assets is large. Second, PG-DPO-Align mitigates this by applying a soft penalty that nudges the policy toward Pontryagin’s ideal controls, thereby enhancing stability and speed of convergence. Third, PG-DPO-OneShot offers an effective shortcut: after briefly training the policy, one can directly compute Pontryagin-aligned controls from backpropagation-derived costates, often achieving far more accurate results (up to 100–1,000 times smaller error) at the cost of not retaining an explicit neural policy in deployment. Fourth, the combined PG-DPO-Align-OneShot method merges both ideas, yielding stable training (thanks to alignment) and rapid, Pontryagin-driven inference (via one-shot).

Taken together, our results demonstrate that neural-network-based stochastic control can indeed manage high-dimensional, continuous-time portfolio optimization *with* consumption. The adjoint-based framework circumvents the curse of dimensionality that plagues standard dynamic programming, enabling tractable solutions for thousands of risky assets. In practice, this opens the door to realistic, large-scale portfolio problems—complete with continuous consumption—while

preserving analytical rigor via Pontryagin’s principle.

These findings also point to several promising directions for future work. First, although we focus on wealth as the core state variable, the framework naturally accommodates additional economic factors such as stochastic volatility, labor income, or macroeconomic indicators. Second, constraints and market frictions—including borrowing limits, transaction costs, and short-selling restrictions—can be incorporated by modifying the forward SDE and Pontryagin Hamiltonian, while retaining the same adjoint-based solution procedure. Third, empirical calibration by fitting the drift and covariance structures to real-world data (possibly time-varying) would more tightly align the method with actual markets and provide richer, data-driven portfolio models. Finally, alternative preferences that extend beyond CRRA to accommodate different utility forms or risk measures (e.g., habit formation, ambiguity aversion) require only small changes to the policy-optimization logic.

Overall, combining Pontryagin’s principle with modern neural backpropagation yields a robust, scalable solver for dynamic portfolio choice in continuous time. By demonstrating feasibility for up to 10,000 (and potentially more) risky assets—and achieving near-optimal performance within mere minutes of training—the hope is that this approach will spur further advances in realistic, data-driven portfolio models and better capture the complexities of global financial markets.

Acknowledgments

Jeonggyu Huh received financial support from the National Research Foundation of Korea (Grant No. NRF-2022R1F1A1063371). This work was supported by the National Research Foundation of Korea (NRF) grant funded by the Korea government (MSIT) (RS-2024-00355646).

References

- Balduzzi, P. & Lynch, A. W. (1999). Transaction costs and predictability: Some utility cost calculations. *Journal of Financial Economics*, 52(1), 47–78. 1
- Borkar, V. S. & Borkar, V. S. (2008). *Stochastic approximation: a dynamical systems viewpoint*, volume 9. Springer. 4.1
- Brandt, M. W., Goyal, A., Santa-Clara, P., & Stroud, J. R. (2005). A simulation approach to dynamic portfolio choice with an application to learning about return predictability. *The Review of Financial Studies*, 18(3), 831–873. 1, 5
- Buraschi, A., Porchia, P., & Trojani, F. (2010). Correlation risk and optimal portfolio choice. *The Journal of Finance*, 65(1), 393–420. 1

- Campbell, J. Y., Chan, Y. L., & Viceira, L. M. (2003). A multivariate model of strategic asset allocation. *Journal of financial economics*, 67(1), 41–80. 1
- Campbell, J. Y. & Viceira, L. M. (1999). Consumption and portfolio decisions when expected returns are time varying. *The Quarterly Journal of Economics*, 114(2), 433–495. 1, 5
- Campbell, J. Y. & Viceira, L. M. (2001). Who should buy long-term bonds? *American Economic Review*, 91(1), 99–127. 1
- Dai, M., Dong, Y., Jia, Y., & Zhou, X. Y. (2023). Learning merton’s strategies in an incomplete market: Recursive entropy regularization and biased gaussian exploration. *arXiv preprint arXiv:2312.11797*. 1, 5
- Fleming, W. H. & Soner, H. M. (2006). *Controlled Markov processes and viscosity solutions*, volume 25. Springer Science & Business Media. 3
- Garlappi, L. & Skoulakis, G. (2010). Solving consumption and portfolio choice problems: The state variable decomposition method. *The Review of Financial Studies*, 23(9), 3346–3400. 1
- Han, J., Jentzen, A., & E, W. (2018). Solving high-dimensional partial differential equations using deep learning. *Proceedings of the National Academy of Sciences*, 115(34), 8505–8510. 1, 5
- Huh, J. (2024). A pontryagin-guided neural policy optimization framework for merton’s portfolio problem. *arXiv preprint arXiv:2412.13101*. 4, 4.5.2, 5.2, 5.2
- Jurek, J. W. & Viceira, L. M. (2011). Optimal value and growth tilts in long-horizon portfolios. *Review of Finance*, 15(1), 29–74. 1
- Kim, T. S. & Omberg, E. (1996). Dynamic nonmyopic portfolio behavior. *The Review of Financial Studies*, 9(1), 141–161. 1
- Kushner, H. J. & Yin, G. G. (2003). *Stochastic Approximation and Recursive Algorithms and Applications*. New York: Springer Science & Business Media. 4.1
- Liu, J. (2007). Portfolio selection in stochastic environments. *The Review of Financial Studies*, 20(1), 1–39. 1
- Lynch, A. W. (2001). Portfolio choice and equity characteristics: Characterizing the hedging demands induced by return predictability. *Journal of Financial Economics*, 62(1), 67–130. 1

- Lynch, A. W. & Balduzzi, P. (2000). Predictability and transaction costs: The impact on rebalancing rules and behavior. *The Journal of Finance*, 55(5), 2285–2309. 1, 5
- Ma, J. & Yong, J. (1999). *Forward-backward stochastic differential equations and their applications*. Number 1702. Springer Science & Business Media. 3.2
- Merton, R. C. (1969). Lifetime portfolio selection under uncertainty: The continuous-time case. *The review of Economics and Statistics*, (pp. 247–257). 1
- Merton, R. C. (1971). Optimum consumption and portfolio rules in a continuous-time model. *Journal of Economic Theory*, 3(4), 373–413. 1, 2
- Pardoux, E. & Peng, S. (1990). Adapted solution of a backward stochastic differential equation. *Systems & control letters*, 14(1), 55–61. 3
- Pham, H. (2009). *Continuous-time stochastic control and optimization with financial applications*, volume 61. Springer Science & Business Media. 3
- Pontryagin, L. S. (2018). *Mathematical theory of optimal processes*. Routledge. 3
- Raissi, M., Perdikaris, P., & Karniadakis, G. E. (2019). Physics-informed neural networks: A deep learning framework for solving forward and inverse problems involving nonlinear partial differential equations. *Journal of Computational physics*, 378, 686–707. 1, 5
- Reppen, A. M. & Soner, H. M. (2023). Deep empirical risk minimization in finance: Looking into the future. *Mathematical Finance*, 33(1), 116–145. 5
- Reppen, A. M., Soner, H. M., & Tissot-Daguette, V. (2023). Deep stochastic optimization in finance. *Digital Finance*, 5(1), 91–111. 5
- Samuelson, P. A. (1975). Lifetime portfolio selection by dynamic stochastic programming. *Stochastic optimization models in finance*, (pp. 517–524). 1
- Weinan, E. (2017). A proposal on machine learning via dynamical systems. *Communications in Mathematics and Statistics*, 1(5), 1–11. 1, 5
- Yong, J. & Zhou, X. Y. (2012). *Stochastic controls: Hamiltonian systems and HJB equations*, volume 43. Springer Science & Business Media. 3.2